ISSN 1674-1056
http://cpb.iphy.ac.cn
http://iopscience.iop.org/cpb
中国物理 B
Chinese Physics
中国物理
Chinese Physics B

High performance InAlN/GaN high electron mobility transistors for low voltage applications

Minhan Mi(宓珉瀚), Meng Zhang(张濛), Sheng Wu(武盛), Ling Yang(杨凌), Bin Hou(侯斌), Yuwei Zhou(周雨威), Lixin Guo(郭立新), Xiaohua Ma(马晓华), Yue Hao(郝跃)
Citation: Chin. Phys. B . 2020, 29(5): 057307 . **doi:** 10.1088/1674-1056/ab821e
Journal homepage: http://cpb.iphy.ac.cn; http://iopscience.iop.org/cpb

What follows is a list of articles you may be interested in

Electronic synapses based on ultrathin quasi-two-dimensional gallium oxide memristor

Shuopei Wang(王硕培), Congli He(何聪丽), Jian Tang(汤建), Rong Yang(杨蓉), Dongxia Shi(时东霞), Guangyu Zhang(张广宇)
Chin. Phys. B . 2019, 28(1): 017304 . **doi:** 10.1088/1674-1056/28/1/017304

Investigation and active suppression of self-heating induced degradation in amorphous InGaZnO thin film transistors

Dong Zhang(张东), Chenfei Wu(武辰飞), Weizong Xu(徐尉宗), Fangfang Ren(任芳芳), Dong Zhou(周东), Peng Yu(于芃), Rong Zhang(张荣), Youdou Zheng(郑有炓), Hai Lu(陆海)
Chin. Phys. B . 2019, 28(1): 017303 . **doi:** 10.1088/1674-1056/28/1/017303

Multi-carrier transport in $ZrTe_5$ film

Fangdong Tang(汤方栋), Peipei Wang(王培培), Peng Wang(王鹏), Yuan Gan(甘远), Le Wang(王乐), Wei Zhang(张威), Liyuan Zhang(张立源)
Chin. Phys. B . 2018, 27(8): 087307 . **doi:** 10.1088/1674-1056/27/8/087307

Simulation study of InAlN/GaN high-electron mobility transistor with AlInN back barrier

Tie-Cheng Han(韩铁成), Hong-Dong Zhao(赵红东), Lei Yang(杨磊), Yang Wang(王杨)
Chin. Phys. B . 2017, 26(10): 107301 . **doi:** 10.1088/1674-1056/26/10/107301

Topological transport in Dirac electronic systems: A concise review

Hua-Ding Song(宋化鼎), Dian Sheng(盛典), An-Qi Wang(王安琦), Jin-Guang Li(李金光), Da-Peng Yu(俞大鹏), Zhi-Min Liao(廖志敏)
Chin. Phys. B . 2017, 26(3): 037301 . **doi:** 10.1088/1674-1056/26/3/037301

High performance InAlN/GaN high electron mobility transistors for low voltage applications*

Minhan Mi(宓珉瀚)[1,†], Meng Zhang(张濛)[1,‡], Sheng Wu(武盛)[1], Ling Yang(杨凌)[2], Bin Hou(侯斌)[1], Yuwei Zhou(周雨威)[2], Lixin Guo(郭立新)[3], Xiaohua Ma(马晓华)[1], and Yue Hao(郝跃)[1]

[1] *Key Laboratory of Wide Band-Gap Semiconductor Materials and Devices, School of Microelectronics, Xidian University, Xi'an* 710071, *China*
[2] *School of Advanced Materials and Nanotechnology, Xidian University, Xi'an* 710071, *China*
[3] *School of Physics and Optoelectronic Engineering, Xidian University, Xi'an* 710071, *China*

(Received 25 February 2020; revised manuscript received 16 March 2020; accepted manuscript online 23 March 2020)

A high performance InAlN/GaN high electron mobility transistor (HEMT) at low voltage operation (6–10 V drain voltage) has been fabricated. An 8 nm InAlN barrier layer is adopted to generate large 2DEG density thus to reduce sheet resistance. Highly scaled lateral dimension (1.2 μm source–drain spacing) is to reduce access resistance. Both low sheet resistance of the InAlN/GaN structure and scaled lateral dimension contribute to an high extrinsic transconductance of 550 mS/mm and a large drain current of 2.3 A/mm with low on-resistance (R_{on}) of 0.9 Ω·mm. Small signal measurement shows an f_T/f_{max} of 131 GHz/196 GHz. Large signal measurement shows that the InAlN/GaN HEMT can yield 64.7%–52.7% (V_{ds} = 6–10 V) power added efficiency (PAE) associated with 1.6–2.4 W/mm output power density at 8 GHz. These results demonstrate that GaN-based HEMTs not only have advantages in the existing high voltage power and high frequency rf field, but also are attractive for low voltage mobile compatible rf applications.

Keywords: InAlN/GaN, high electron mobility transistor (HEMT), low voltage

PACS: 73.50.–h, 73.61.–r, 85.90.+h **DOI:** 10.1088/1674-1056/ab821e

1. Introduction

Owing to its high mobility and high electron saturation velocity, GaN-based high electron mobility transistors (HEMTs) have great potential in rf applications.[1–4] Up to date, the main focus on GaN-based HEMTs is their large output power performance at high operation voltage[5,6] and high frequency characteristics.[7–9] However, Intel reports that GaN-based HEMTs have superior performance than Si and GaAs devices at high voltage operation, at low operating voltage GaN-based HEMTs have lower R_{on} than Si-based transistors at the same breakdown voltage (V_{br}), and have advantages over GaAs rf devices in terms of efficiency and output power.[10] These results signify that the applications of GaN-based HEMTs can extend from the existing high voltage operation into low voltage mobile compatible rf operation modes. For GaN-based high voltage rf devices, one of the most commonly used methods to improve the output power is to increase the operating voltage through the adoption of field plate, back barrier and other technologies.[11–15] However, for low voltage applications, due to the limitation of operating voltage, the drain voltage applied to the device is generally limited to a fixed lower range, thus the methods of output power improvement are totally different, which can only be obtained by minimizing the parasitic resistance, knee voltage and increasing the output current.

In this paper, due to the strong spontaneous polarization, the InAlN/GaN heterojunction has larger 2DEG than conventional AlGaN/GaN,[16] thus enables the use of thinner barrier thickness (below 10 nm) while obtaining higher 2DEG (1.7×10^{13} cm^{-2}).[17,18] Therefore, based on the advantages in the InAlN/GaN structure, firstly we adopt an 8-nm-thick InAlN barrier to simultaneously obtain large 2DEG density and to suppress the short channel effect. The large 2DEG density could effectively reduce parasitic resistance, which contributes to output power enhancement.[19] The suppressed short channel effect on the one hand could enable higher frequency operation, which makes the device have a higher gain at a specific frequency, and on the other hand it makes the device to exhibit good pinch-off characteristics, which are necessary for power added efficiency.[20] Secondly, the source–drain spacing is reduced to 1.2 μm to further decrease parasitic resistance, so as to further enhance the output current and to lower the knee voltage. In addition, a SiN passivation layer with a T-shaped gate structure, which is commonly used in microwave power device, is adopted to suppress current collapse and knee voltage walkout that is related to output power and power added efficiency performance.[21] The fabricated low-voltage InAlN/GaN HEMT shows a maximum out-

*Project supported by the China Postdoctoral Science Foundation (Grant No. 2018M640957), the Fundamental Research Funds for the Central Universities, China (Grant No. 20101196761), the National Natural Science Foundation of China (Grant No. 61904135), the National Defense Pre-Research Foundation of China (Grant No. 31513020307), and the Natural Science Foundation of Shaanxi Province of China (Grant No. 2020JQ-316).

†Corresponding author. E-mail: miminhan@qq.com
‡Corresponding author. E-mail: 498078211@qq.com

© 2020 Chinese Physical Society and IOP Publishing Ltd

put current of 2.3 A/mm with R_{on} of 0.9 Ω·mm, a maximum extrinsic transconductance of 550 mS/mm, a current collapse of 9%. From small-signal measurement, the f_T/f_{max} is estimated to be 131 GHz/196 GHz. At the operating frequency of 8 GHz, 64.7%–52.7% PAE associated with 1.6–2.4 W/mm output power density is achieved at V_{ds} = 6–10 V. It exhibits excellent power performance in the low-voltage operation.

2. Device structure and fabrication

A schematic diagram of the InAlN/GaN HEMT is presented in Fig. 1(a). The heterostructure was grown on a SiC substrate by metal organic chemical vapor deposition (MOCVD), consisting of a 1.2 μm GaN buffer layer, a 1 nm AlN spacer layer, and an 8 nm $In_{0.17}Al_{0.83}$ N barrier layer. The hall measurements showed a carrier density of 1.7×10^{13} cm^{-2} and sheet resistance of 220 Ω /□ at room temperature.

The device fabrication started with the formation of source and drain ohmic consisting of Ti/Al/Ni/Au metals deposited by electron beam evaporation and annealed at 780 ℃ for 30 s in N_2 ambient. Afterwards, the device isolation was achieved by using Boron implantation. The ohmic contact resistance was 0.25 Ω·mm by using transmission line measurement (TLM). A 120 nm SiN passivation layer was deposited by plasma enhanced chemical vapor deposition (PECVD), and the E-beam lithography (EBL) was adopted to define gate foot. As shown in Fig. 1(b), the 0.15 μm gate foot was opened by CF_4-based etching to remove SiN. Finally, the gate head based on Ni/Au/Ni metals was deposited by electron beam evaporation as shown in Fig. 1(b). The T-shaped gate was formed with the gate length of 0.15 μm, and the gate head of 0.75 μm. The source-drain distance was 1.2 μm.

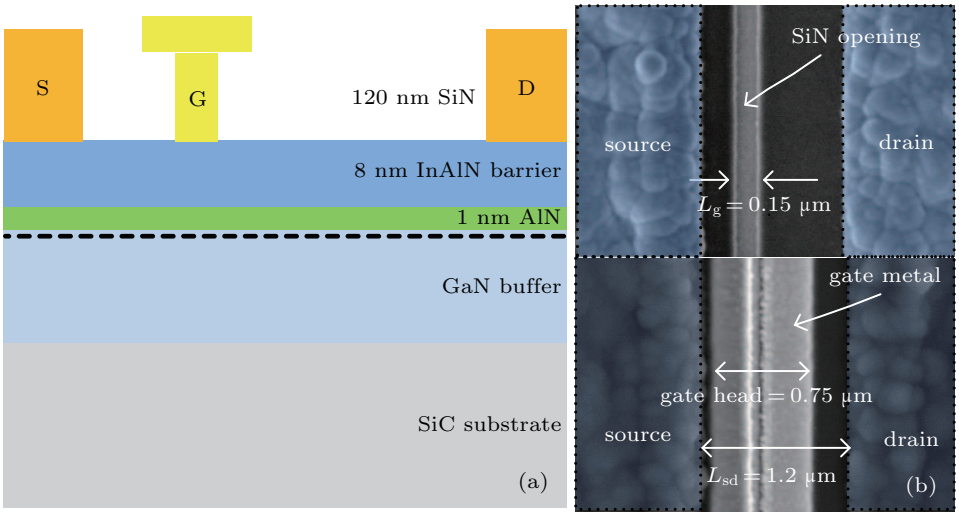


Fig. 1. (a) Cross section of the InAlN/GaN HEMT. (b) SEM graph of the fabricated InAlN/GaN in the top view.

3. Results and discussion

A Keithley 4200 semiconductor parameter analyzer was used for both dc and pulse measurement of the InAlN/GaN HEMT. Figure 2 shows the transfer characteristics of the device at V_{ds} = 6 V. The threshold voltage (V_{th}) in this study is defined as the gate bias intercept of the linear extrapolation of drain current at the peak transconductance. The V_{th} of this device is −4 V, and peak extrinsic transconductance is 550 mS/mm. The device shows the on/off ratio over 5×10^5, and sub-threshold swing (SS) of 120 mV/decade.

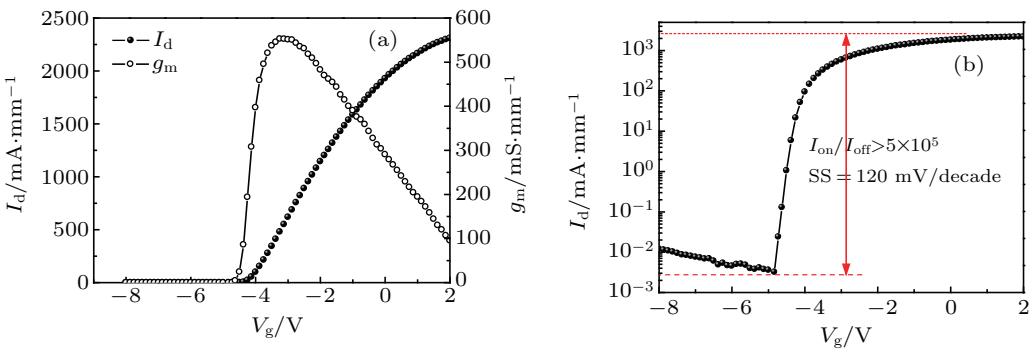


Fig. 2. (a) Transfer characteristics of the InAlN/GaN HEMT in linear coordinates. (b) Transfer characteristics of the InAlN/GaN HEMT in semi-log coordinates.

Figure 3(a) shows the output characteristics of the InAlN/GaN HEMT. The maximum output current of 2.3 A/mm was measured at $V_{gs} = 2$ V with R_{on} of 0.9 Ω·mm. The large drain current and lower R_{on} are attributed to lower sheet resistance and scaled source-drain dimension. In addition, a small output conductance at all gate bias range is attributed to the enhanced aspect ratio. These findings indicate that the InAlN/GaN HEMT has excellent gate control ability and the short channel effect is well suppressed. Figure 3(b) shows the gate leakage of the InAlN/GaN HEMT. It is observed that the gate leakage is lower than 1 mA/mm at $V_{gs} = 2$ V, indicating that the gate voltage of 2 V applied to gate is applicable, which is helpful for improving the output current.

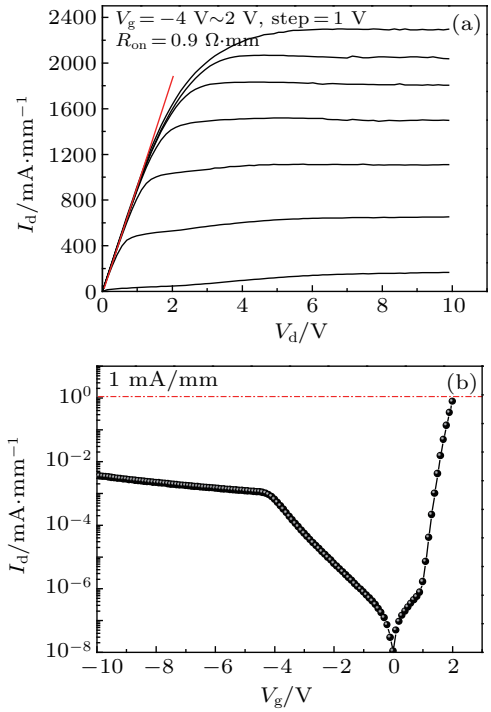


Fig. 3. (a) Output characteristics of the InAlN/GaN HEMT. (b) Schottky characteristics of the InAlN/GaN HEMT.

Figure 4(a) shows the pulsed *I*–*V* characteristics of the InAlN/GaN HEMT, where the quiescent bias points are chosen at $(V_{GSQ}, V_{DSQ}) = (0\ \text{V}, 0\ \text{V})$ and $(V_{GSQ}, V_{DSQ}) = (-8\ \text{V}, 10\ \text{V})$. The pulse period and width are 10 μs and 0.5 μs, respectively. The current collapse ratio is about 9%, which enables the rf output current capacity. In this paper, the breakdown voltage is defined as the drain voltage (V_{br}) that the drain current reaches 1 mA/mm at which gate voltage is biased at −8 V. The V_{br} of the InAlN/GaN HEMT is 33 V as shown in Fig. 4(b). Obviously, the breakdown is caused by gate leakage.

The *S* parameter was measured using an Agilent8363B network analyzer in the frequency range 1–40 GHz with a short-open-load-through calibration. The f_T and f_{max} were measured by biasing the device at the maximum g_m point ($V_{gs} = -3$ V) for $V_{ds} = 8$ V. By extrapolating the short circuit current gain (H_{21}) and the maximum stable gain (MSG) curves using −20 dB/decade slopes, f_T and f_{max} of the InAlN/GaN HEMT are 131 GHz and 196 GHz. The small-signal performance can fully meet the requirement of 5 G applications. Power performance at 8 GHz was measured in continuous wave using an on-wafer load-pull system. Figure 6(a) shows power sweep of the InAlN/GaN HEMT, which is biased at class AB operation at $V_{ds} = 8$ V. The PAE was 60%, with output power density of 2.1 W/mm and power gain of 13.3 dB. Figure 6(b) shows the output power density and the PAE versus the drain voltage. The output power density of 1.6–2.4 W/mm associated with 64.7%–52.7% PAE at drain voltage varies from 6 V to 10 V. We notice that the device in Ref. [10] was measured at 2 GHz, demonstrating power density of 0.55 W/mm combined with PAE of 80%, and in Ref. [20] was measured at 10 GHz, demonstrating

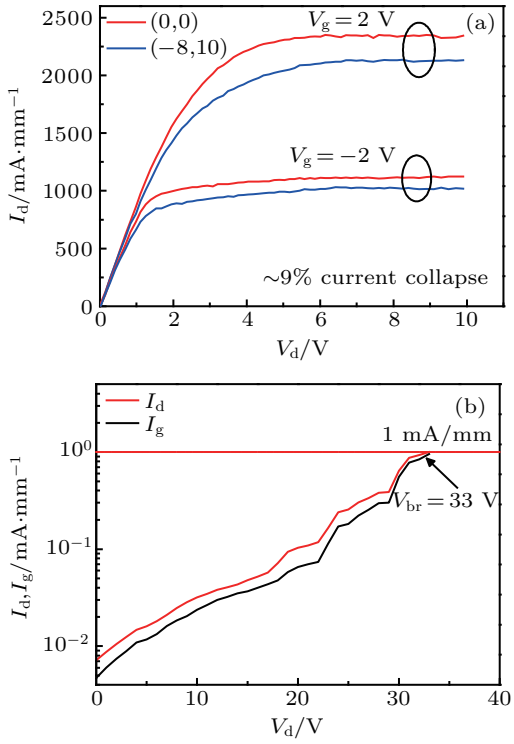


Fig. 4. (a) Pulsed *I*–*V* characteristics of InAlN/GaN HEMT. (b) Off-state breakdown characteristics of InAlN/GaN HEMT.

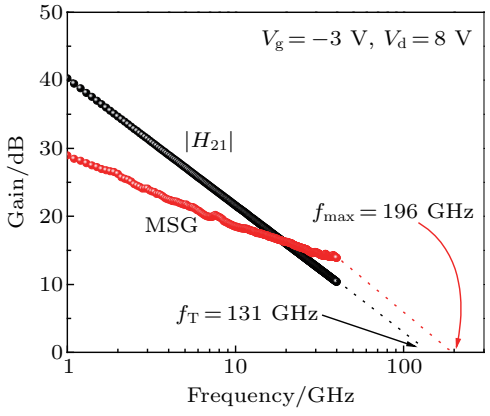


Fig. 5. Small-signal characteristics of InAlN/GaN HEMT.

power density of 2 W/mm associated with PAE of 60%. Compared with the devices measured at adjacent frequency, the power performance of device fabricated in this paper is in relative advanced level among the low voltage range. The excellent power performance at low drain voltage operation can be attributed to the high output current and lower knee voltage. The reasons for high output current and lower knee voltage are strong spontaneous polarization InAlN barrier induced large 2DEG density and smaller source–drain spacing induced lower parasitic resistance.

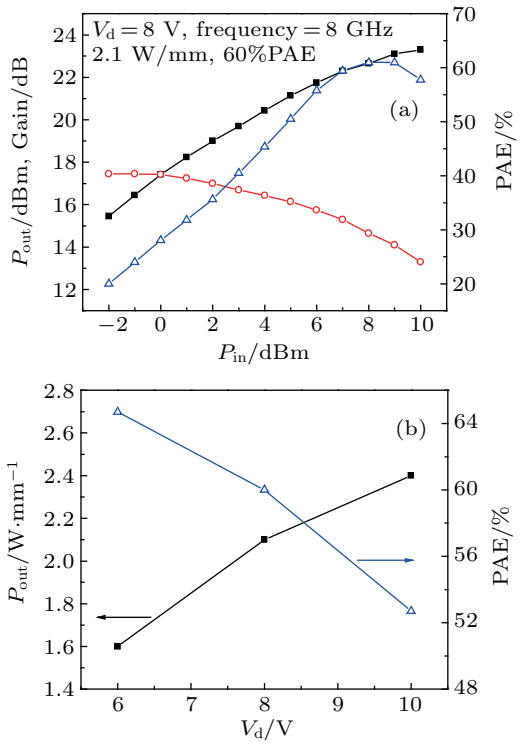


Fig. 6. (a) Large signal characteristics of the InAlN/GaN HEMT at 8 GHz. (b) Output power and power added efficiency versus drain voltage at 8 GHz.

4. Conclusion

In summary, an InAlN/GaN HEMT with scaled lateral dimension has been fabricated for high performance low voltage applications. Depending on the strong polarization induced high 2DEG of the InAlN/GaN structure, a thin barrier layer can be used simultaneously to obtain low sheet resistance and to suppress the short channel effect. A highly scaled lateral dimension reduces the access resistance. Measurements show that the fabricated device exhibits very high drain current of 2.3 A/mm accompanied by the R_{on} of 0.9 Ω·mm. The improved on-state characteristic is attributed to the low sheet resistance and the scaled lateral dimension. In addition, the on/off ratio over 5×10^5 and SS of 120 mV/decade indicate that the short channel effect is well suppressed. At 8 GHz, the InAlN/GaN HEMT shows output power density of 1.6–2.4 W/mm associated with 64.7%–52.7% PAE at drain voltage varying from 6 V to 10 V. These results show that GaN-based HEMTs are attractive in low voltage and low power field as well as high voltage and high frequency field.

References

[1] Wu S B, Gao J F, Wang W B and Zhang J Y 2016 *IEEE Trans. Electron. Devices* **63** 3882

[2] Hao Y, Yang L, Ma X H, Ma J G, Cao M Y, Pan C Y, Wang C and Zhang J C 2011 *IEEE Electron Device Lett.* **32** 626

[3] Yang L, Zhou X W, Ma X H, Lv L, Cao Y R, Zhang J C and Hao Y 2017 *Chin. Phys. B* **26** 017304

[4] Mi M H, Ma X H, Yang L, Lu Yang, Hou B, Zhu J J, Zhang M, Zhang H S, Zhu Q, Yang L A and Hao Y 2017 *IEEE Trans. Electron. Devices* **64** 4875

[5] Palacios T, Chakraborty A, Rajan S, Poblenz C, Keller S, DenBaars S P, Speck J S and Mishra U K 2005 *IEEE Electron Device Lett.* **26** 781

[6] Chu R M, Shen L, Fichtenbaum N, Brown D, Chen Z, Keller S, DenBaars S P and Mishra U K 2008 *IEEE Electron Device Lett.* **29** 974

[7] Yue Y Z, Hu Z Y, Guo J, Sensale-Rodriguez B, Li G W, Wang R H, Faria F, Fang T, Song B, Gao X, Guo S P, Kosel T, Snider G, Fay P, Jena D and Xing H L 2012 *IEEE Electron Device Lett.* **33** 988

[8] Shinohara K, Regan D C, Tang Y, Corrion A L, Brown D F, Wong J C, Robinson J F, Fung H H, Schmitz A, Oh T C, Kim S J, Chen P S, Nagele R G, Margomenos A D and Micovic M 2013 *IEEE Trans. Electron. Devices* **60** 2982

[9] Mi M H, Ma X H, Yang L, Lu Y, Hou B, Zhang M, Zhang H S, Wu S and Hao Y 2019 *AIP Adv.* **9** 045212

[10] Then H W, Chow L A, Dasgupta S, Gardner S, Radosavljevic M, Rao V R, Sung S H, Yang G and Chau R S 2015 *Proceedings of Symposium on VLSI Technology*, June 16–18, 2015, Kyoto, Japan, p. 202

[11] Mao W, Fan J S, Du M, Zhang J F, Zheng X F, Wang C, Ma X H, Zhang J C and Hao Y 2016 *Chin. Phys. B* **25** 127305

[12] Ando Y, Okamoto Y, Miyamoto H, Nakayama T, Inoue T and Kuzuhara M 2003 *IEEE Electron Device Lett.* **24** 289

[13] Wu Y F, Saxler A, Moore M, Smith R P, Sheppard S, Chavarkar P M, Wisleder T, Mishra U K and Parikh 2004 *IEEE Electron Device Lett.* **25** 117

[14] Liu J, Zhou Y, Zhu J, Cai Y, Lau K M and Chen K J 2007 *IEEE Trans. Electron. Devices* **54** 2

[15] Tsou C W, Kang H C, Lian Y W and Hsu S 2016 *IEEE Trans. Electron. Devices* **63** 4218

[16] Medjdoub F, Alomari M, Carlin J F, Gonschorek M, Feltin E, Py M A, Grandjean N and Kohn E 2008 *IEEE Electron Device Lett.* **29** 422

[17] Crespo A, Bellot M M, Chabak K D, Gillespie J K, Jessen G H, Miller V, Trejo M, Via G D, Walker D E, Jr, Winningham B W, Smith H E, Cooper T A, Gao X and Guo S 2010 *IEEE Electron Device Lett.* **31** 2

[18] Chung J W, Saadat O I, Tirado J M, Gao X, Guo S P and Palacios T 2009 *IEEE Electron Device Lett.* **30** 904

[19] Lu Y, Ma X H, Yang L, Hou B, Mi M H, Zhang M, Zheng J X, Zhang H S and Hao Y 2018 *IEEE Electron Device Lett.* **39** 811

[20] Saunier P, Schuette M L, Chou T M, Tserng H Q, Ketterson A, Beam E, Pilla M and Gao X 2013 *IEEE Trans. Electron. Devices* **60** 3099

[21] Vetury R, Zhang N Q, Keller S and Mishra U K 2001 *IEEE Trans. Electron. Devices* **48** 560